Synthesis of Composite Nanosheets of Graphene and Boron Nitride and Their Lubrication Application in Oil

*Yuchen Liu, Srikanth Mateti, Chao Li, Xuequan Liu, Alexey M. Glushenkov, Dan Liu, Lu Hua Li, Daniel Fabijanic, and Ying Chen**

Composite nanosheets of graphene and boron nitride have been produced in large quantities for the first time using high-energy ball milling in ammonia gas as an exfoliation agent. The anti-wear properties of the composite nanosheets as a lubricant additive are investigated via a four-ball method. The results show that the composite nanosheets are exfoliated from the commercial graphite and h-BN powders and combined into graphene/BN composite nanosheets during the ball milling process. The composite nanosheets formed have diameters larger than 200 nm and consist of heterostructures of approximately 10 monolayers of graphene and BN. The composite nanosheets exhibit better wear resistance and friction reduction properties than the homogeneous nanosheets because of the stronger interaction between graphene and BN nanosheets, which can effectively improve the anti-wear properties of mineral base oil as a lubricant additive.

1. Introduction

Since graphene was discovered in 2004,[1] it has attracted considerable attention due to extraordinary physical and mechanical properties, such as high surface area, high Young's modulus, and high thermal conductivity.[2,3] Similarly, 2D structural analogs including hexagonal boron nitride (h-BN) nanosheets and transition metal dichalcogenides (TMDs) nanosheets also have exhibited many distinct properties,[4–11] affording a wide potential application range.[12–15]

Two dimensional nanosheets offer many advantages in tribological applications. Their layered structure consists of strong sp^2 covalent in-plane bonds and weak Van der Waals interlayer bonds, which facilitates inter-plane sliding and low friction. Further, the flake morphology allows penetration and stable deposition into the rubbing area, avoiding direct contact between the sliding surfaces. As additives, these features conspire to significantly improve the anti-wear and friction-reducing lubrication performance of oil.[16–20] Huang et al. reported an over 50% reduction in wear scar diameter and reduced coefficient of friction (0.06–0.08 μ to 0.01–0.02 μ) for paraffin oil containing graphene, relative to natural flake graphite powder additives.[21] Due to the hybridization of different material properties, composite nanosheets of graphene and BN nanosheets may overcome the limitations of graphene. In particular, BN nanosheets have higher thermal and chemical stability than graphene and very different surface property. Both materials are well-known lubricants, however, their composites have not been previously studied as lubricants. This requires experimental verification and is the focus of this present work.

Chemical vapor deposition (CVD),[22] hydrothermal,[23] and mechanical transfer[24] methods can be used to produce various composite nanosheets on substrate surfaces at a small scale. However, synthesis of a large quantity of composite nanosheets is still a considerable challenge. Recently, controlled ball milling using ammonia or hydrocarbon gases, as exfoliation agents has been found to be an efficient and high yield production method to produce pure nanosheets of graphene, BN, MoS_2, and WS_2.[25] In this process, the obtained nanosheets remained flat and maintained their single-crystalline structure with a low defect density, even after a long period of milling. During the ball milling process, NH_3 and C_2H_4 molecules were chemically adsorbed on the nanosheet surfaces and acted as a lubricant to reduce the milling impact on the nanosheets. The gas molecules attached at edge and defect sites underwent chemical reactions and healed the defects by saturating the dangling bonds.[25]

In this study, an optimized high-energy ball milling process was employed for the first time to produce composite nanosheets of graphite and boron nitride. The wear resistance and friction reducing the performance of the composite nanosheets, as a lubricant additive were evaluated via a four-ball method.

2. Results and Discussion

2.1. Composite Nanosheet Synthesis

Figure 1 shows the XRD spectra of graphite and BN powder mixtures milled for different periods of time. After being ball

Prof. Y. Chen, Dr. Y. Liu, Dr. S. Mateti, Dr. A. M. Glushenkov, Dr. D. Liu, Dr. L. H. Li, Dr. D. Fabijanic
Institute for Frontier Materials
Deakin University, Geelong, 3216, Australia
E-mail: ian.chen@deakin.edu.au

Dr. C. Li, Prof. X. Liu
Powder Metallurgy Department
Central Iron and Steel Research Institute, Beijing, 100081, China

The ORCID identification number(s) for the author(s) of this article can be found under https://doi.org/10.1002/adem.201700488.

DOI: 10.1002/adem.201700488

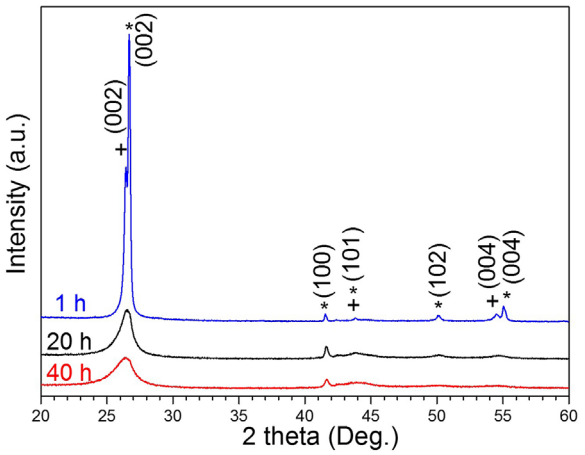

Figure 1. XRD patterns of BN and graphite with different milling times, +: graphite, *: BN.

milled for 1 h, the XRD spectra of the graphite and BN mixture show two strong (002) characteristic peaks between 26° and 27°. By referring to the XRD spectra of commercial graphite and BN, the peaks located at 26.5°and 54.5° can be identified as originating from graphite, and the peaks at 26.7° and 56° belong to h-BN phase. With increasing milling time, the characteristic peaks of hexagonal structures ((002) and (004)) are weaker and broaden because of particle size reduction, and the (100), (101), and (004) peaks almost vanish. This result suggests that the thickness-to-size ratio of the starting particles were reduced and the nanosheets were exfoliated from bulk materials after ball milling for 20 or 40 h. Additionally, the two individual (002) and (004) peaks combined to one peak, suggesting the homogeneous graphene and BN nanosheets combined into graphene/BN composite nanosheets.

SEM images revealing the morphologies of composite nanosheets synthesized after different ball milling times are shown in **Figure 2**. A thin carbon coating was used to reduce the charging effect from the electrically insulating BN samples. After the BN and graphite mixture was ball milled for 1 h, the particles were thick and blocky, and the diameter was still greater than 2 µm (Figure 2a). However, as the milling time increased, the layered structure was extensively exfoliated. After 20 h of milling, nanosheets with a large surface area and uniform size can be seen clearly in Figure 2b. Multiple composite nanosheets were loosely stacked with distinct edges, and the nanosheets had diameters larger than 200 nm. Extending the milling time to 40 h further reduced the size of individual composite nanosheets to a diameter of ≈100 nm (Figure 2c). These 40 h milled graphene/BN composite nanosheets were compactly stacked together, and loose individual composite nanosheets agglomerated to form clusters. It is known that the starting particles are subjected to shear and fragmentation forces during the ball milling procedure.[26–29] When the shear force exceeds the weak interlayer Van der Waals bonds, the bulk materials exfoliate into nanosheets. Therefore, excessive milling times (e.g., 40 h) results in the reduction in the size of individual nanosheets and causes the nanosheets to agglomerate tightly.

Oleic acid was used in the nanosheet synthesis to enhance the mechanical exfoliation process and improve the dispersion of composite nanosheets in mineral oil. However, the acid may obscure features in SEM imaging. Consequently, the 20 h ball milled graphene/BN composite nanosheets were washed by ultrasonic cleaning in petroleum spirit to remove the oleic acid. Figure 2d shows a SEM image of the graphene/BN composite nanosheets after removing the oleic acid. Relative to Figure 2a, the insulating BN nanosheets (white regions) with a diameter less than 100 nm are distinct and dispersed homogeneously on the dark graphene to form the stacked composite structure.

Twenty hours milled samples were investigated using TEM and EELS to further reveal the microstructure and elemental distribution of the graphene/BN composite nanosheets. **Figure 3**a exhibits an edge of a composite nanosheet suspended

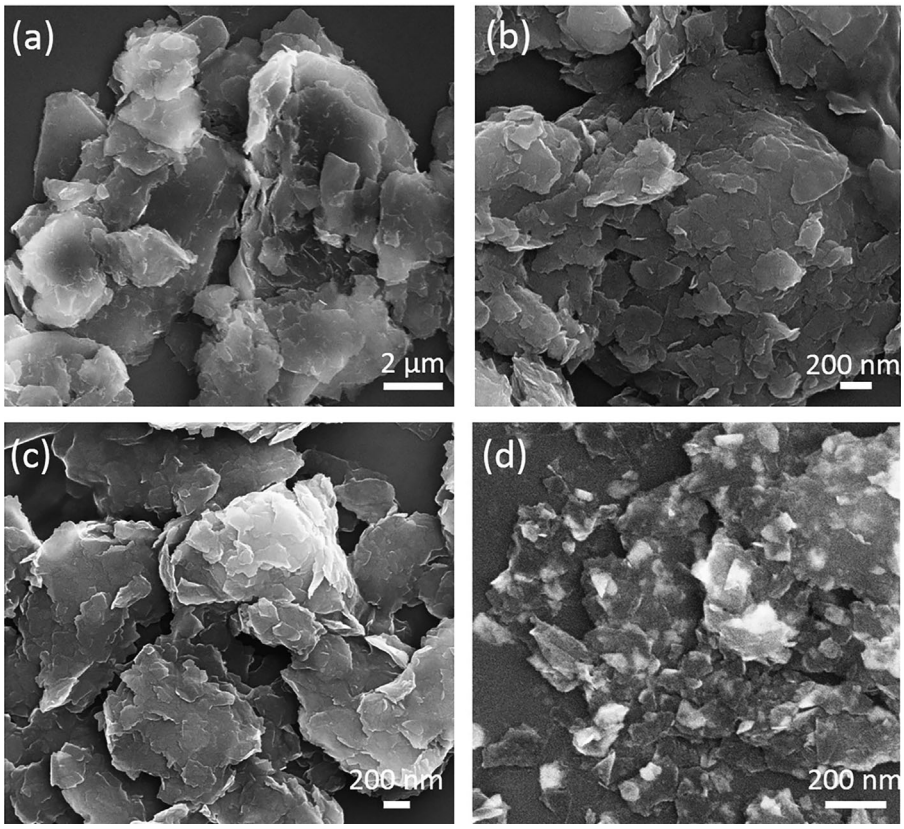

Figure 2. SEM images of the graphite and BN mixture samples milled for different times: a) 1 h; b) 20 h; c) 40 h; d) the 20 h sample without the oleic acid and carbon coating.

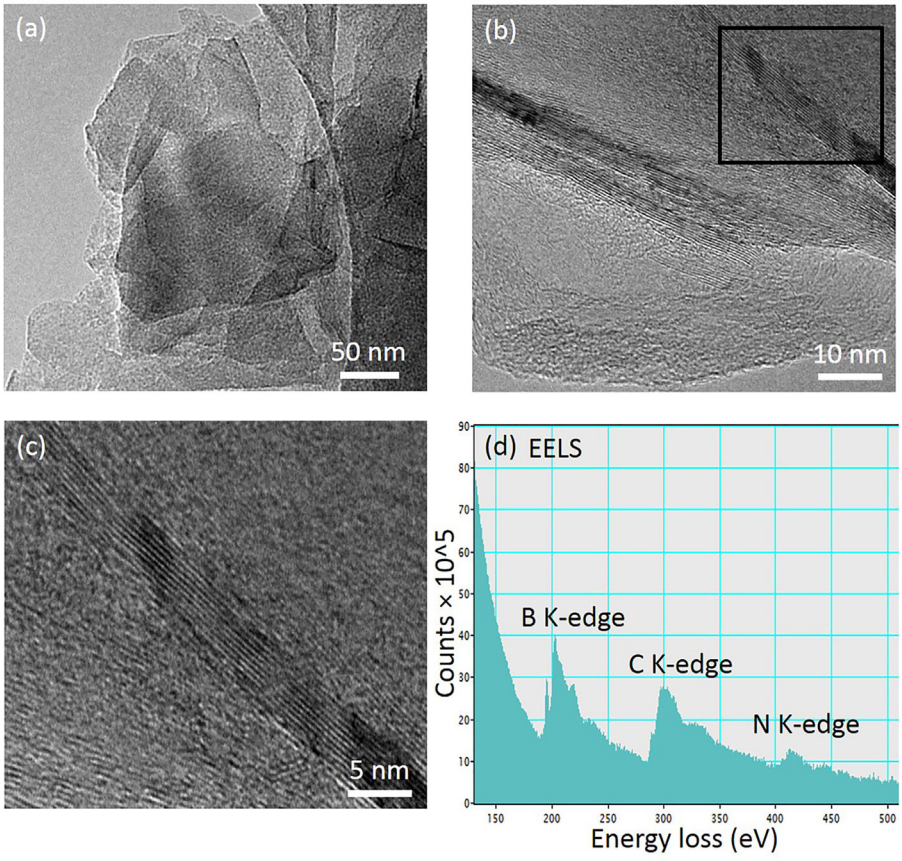

Figure 3. a) TEM images of graphene/BN composite nanosheets produced by ball milling for 20 h; b) high-magnification TEM image; c) enlarged TEM image of the selected area (indicated by the box); d) EELS spectrum of graphene/BN composite nanosheets.

on a holey carbon film. It is apparent that multiple nanosheets were irregularly stacked together and the degree of transparency is indicative of the number of stacked sheets. The thickness of the nanosheets can be estimated from a side view of the structure in a high-magnification TEM image shown in Figure 3b and c. Each individual graphite or BN nanosheets is composed of approximately 10 monolayers of graphene or BN, and the typical thickness of the nanosheets is less than 10 nm. The EELS spectrum in Figure 3d shows the elemental edges of B, C, and N, indicating that the composite nanosheets were formed from BN and graphene.

Energy-filtered TEM (EFTEM) was used to visualize the elemental distribution in a region of the sample suspended over a hole in a holey carbon film (**Figure 4**a). The distribution of elements is shown in an energy-filtered image (Figure 4b), where boron is marked in red and carbon is depicted in green. The individual energy-filtered maps of boron and carbon are displayed in Figure 4c and d. The boron and carbon colored regions are overlapping, but discrete graphene and BN nanosheets can also be identified at the particle edges. It can be concluded that the composite nanosheets are constructed by stacking of multiple graphene and BN nanosheets together.

2.2. Tribology Studies

The wear resistance of graphene/BN composite nanosheets was evaluated via a four-ball method according to the standard ASTM D2783-88. The four-ball method is a common technique to evaluate the load-carrying capacity and abrasion resistance of a lubricant. An upper rotary ball is connected to a transmission, which can apply various loads to three stationary lower balls and the three contact areas are immersed in the testing lubricant. Friction occurs when the upper ball rotates against the lower balls and wear scars are generated during this procedure. After each loading, the wear scar diameter was measured by an ocular micrometer equipped with a calibrated measuring scale (±0.01 mm). Under the same load and rotary speed, a smaller wear scar diameter indicates is and the better friction-reduction of the lubricant will be. The graphene/BN composite nanosheets made by different ball milling times were selected as lubricating additives and then dispersed into mineral base oil at an addition proportion of 1 wt%, which is the common concentration of nanosheets additives selected for testing.[17,21,30,31]

The last nonseizure load (P_B) and weld point (P_D) of the mineral base oil containing nanosheet additives were determined according to ASTM D2783-88 standard procedure. P_B is the last nonseizure load at which the commencement of plastic deformation of the steel balls is observed, and P_D is the weld point at which the fusion between the rubbing metal surfaces occurs. **Figure 5** shows the P_B and P_D values of the neat mineral base oil and the oil containing 1 wt% of the composite nanosheets. It is seen that both P_B and P_D values of the mineral base oil increase significantly (P_B from 255 to 392 N and P_D from 1236 to 1569 N) with 1 wt% composite nanosheets addition. The typical wear scars of the steel balls after testing are shown in **Figure 6**. The wear scar lubricated by the oil with composite nanosheet additive is smaller and smoother compared with that of neat mineral oil (Figure 6). The improvement in wear resistance can be attributed to the composite nanosheets consisting of multiple layers of graphene and BN nanosheets. The ultrathin composite nanosheets can easily be adsorbed on the rubbing surface, which separates the rubbing surface to avoid direct contact. The layered structure and flexibility of the composite nanosheets can facilitate a mending and polishing effect,[32] similar to reports of nanoparticles used to enhance the anti-wear properties of the mineral base oil.

The effects of the size and morphological features of the composite nanosheets resulting from different milling times

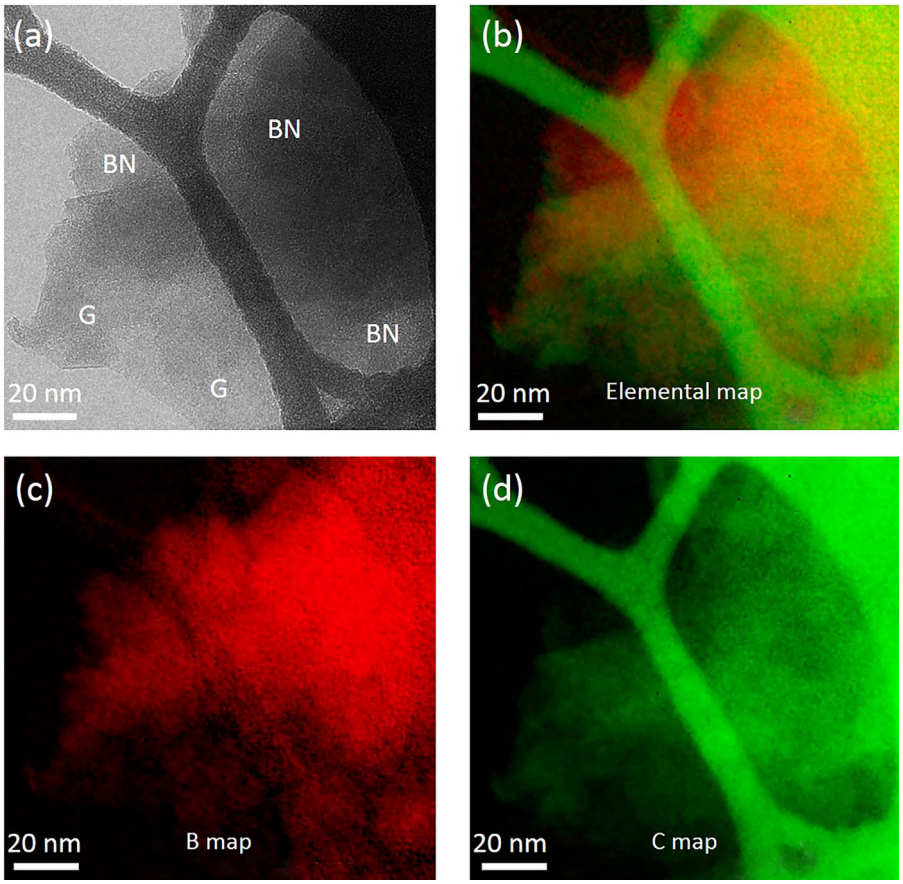

Figure 4. Energy-filtered TEM data: a) an elastic TEM image; b) an energy-filtered image of the same area with elemental contrast (boron–red, carbon–green); c, d) individual energy-filtered maps of boron and carbon.

on the anti-wear properties were investigated. 1 wt% of the graphene/BN composite nanosheets were dispersed into neat mineral base oil and tested by the four-ball method. The wear scar diameters of the testing steel balls in the oils with different additives under varying loads were measured, and the results are plotted in **Figure 7**a. The average wear scar diameters of the mineral base oil containing the composite nanosheets produced by 1 and 20 h ball milling were the largest and the smallest, respectively (Figure 7a). This indicates that the graphene/BN composite nanosheets produced by 20 h ball milling time possess the best anti-wear properties.

The graphene/BN composite powders produced by 1 h ball milling are not layer structured (see Figure 2a), which may restrict particle flow into the contact region and result in the larger wear scar diameters. As the milling time increased to 20 h the layered graphite and h-BN were extensively exfoliated, resulting in a reduced diameter (large than 200 nm) and a thickness of less than 10 nm. This reduced size allowed the nanocomposite to readily enter the gap between rubbing surfaces, as illustrated in **Figure 8**. The layered structure and flexibility of the composite nanosheets can generate the mending effect and the polishing effect,[32,33] so the wear scar diameters of the oil containing the composite nanosheets decreased. When the milling time was further increased to 40 h, the diameter of the graphene/BN composite nanosheets reduced and individual composite nanosheets agglomerated to form large inflexible nanosheets clusters. These clusters act like large particles and have a limited lubrication effect.

To compare to composite nanosheets, homogeneous graphene and BN nanosheets were produced separately by the same optimized (20 h) ball milling process and dispersed at a concentration of 1 wt% into neat mineral base oil. The wear scar diameters of these oil mixtures under six different loads in the range of P_B and P_D were determined in sequence by four-ball method. Figure 7b presents the wear scar diameters of the mineral base oil with and without nanosheet additives. Welding of the steel balls in the rubbing surfaces occurs under a load of 1236 N for the neat mineral base oil, and the wear scar diameters of the mineral base oil containing all nanosheets clearly decrease. The reduction in wear scar diameter of the oil with the composite nanosheets under the same load is more remarkable than those of the oil containing homogeneous nanosheets, which indicates that the composite nanosheets possess the better anti-wear properties. Furthermore, the effect of different nanosheet additives on the friction coefficient of different oils was investigated via the four-ball method. **Figure 9** shows the changes of friction coefficient versus time for neat mineral base oil and mineral base oil containing 1 wt% of three different nanosheets (BN nanosheets, grapheme, and graphene/BN composite nanosheets). It can be seen that the mineral base oil containing graphene/BN composite nanosheets

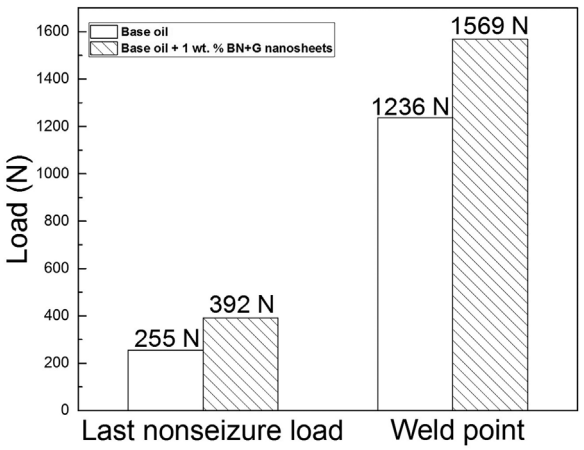

Figure 5. Last nonseizure load and weld point of the base oil and the oil containing graphene/BN composite nanosheets.

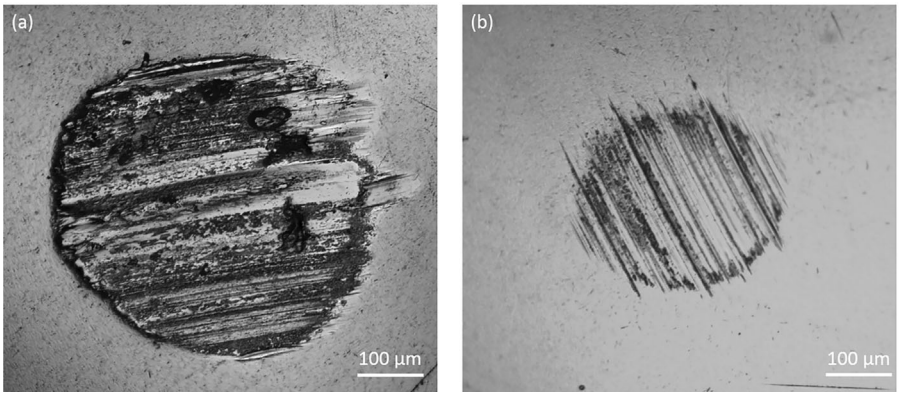

Figure 6. Optical microscopy images of wear scars of the steel balls tested in a) neat base oil and b) base oil with graphene/BN composite nanosheets (four-ball method, 1770 rpm, 392 N, 10 s).

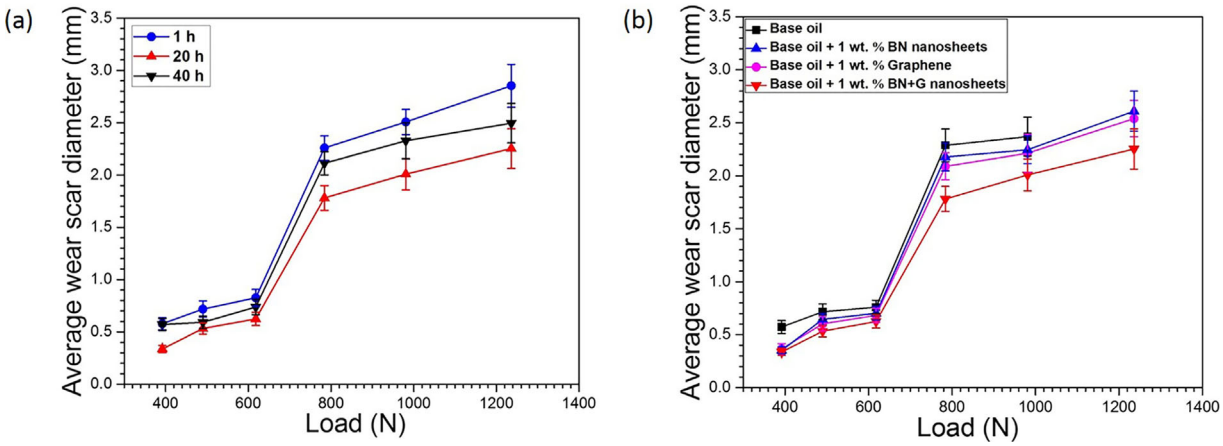

Figure 7. Average diameters of wear scars under different loads in mineral base oils added with the composite nanosheets prepared using different milling times a) and in the oils with different nanosheets b) (four-ball method, 1770 rpm, 10 s).

displays the lowest friction coefficient relative to the neat mineral base oil and mineral base oil containing homogeneous nanosheets.

Different nanosheets exhibit distinct behavior under external pressure. Thin graphene sheets become stronger compared to thicker graphite sheets,[2] whereas the strength of BN nanosheets

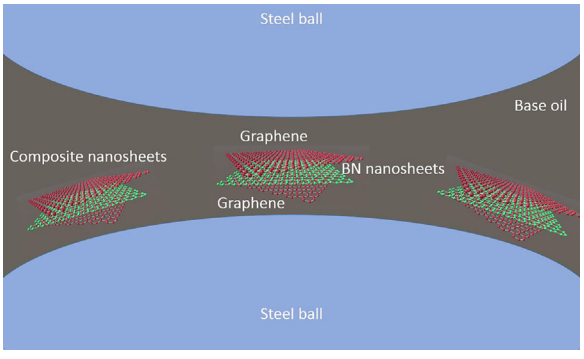

Figure 8. Schematic of possible lubrication mechanism of graphene/BN composite nanosheets as lubricating activities in oils.

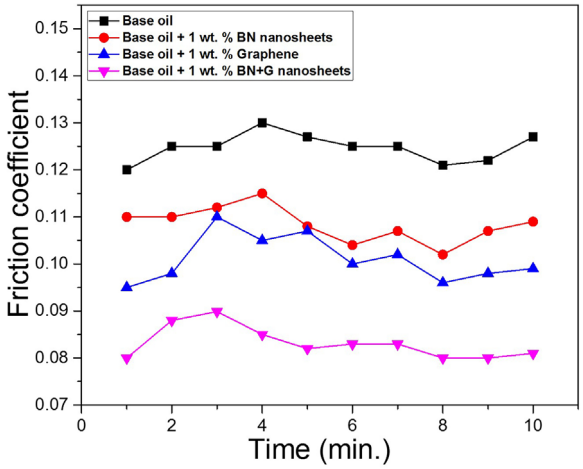

Figure 9. Friction coefficient for the neat base oil and the base oils containing different nanosheets (four-ball method, 1770 rpm, 200 N, 10 min).

is not sensitive to their thickness because of the comparatively stronger interaction between basal planes under applied pressure.[34] Leven et al. have theoretically predicted that a robust superlubricity state occurs between the sliding interface of sufficiently large graphene and BN layers, leading to a low friction state.[35] This fundamental study is consistent with the experimental results of friction coefficients in the present work.

3. Conclusions

Large-scale production of graphene/BN composite nanosheets have been achieved via a high-energy ball milling process conducted on graphite and h-BN powders in an ammonia gas atmosphere. The size and morphologies of the composite nanosheets were influenced by varying the milling time, which subsequently affected the wear resistance. The composite graphene/BN nanosheets produced by 20 h of ball milling time have large diameters and thin thickness, which form a better film on the testing ball surface resulting in a lower friction coefficient and improved anti-wear properties.

4. Experimental Section

The commercial graphite and h-BN powders with diameters of less than 40 μm were chosen as starting particles. An optimized high-energy ball milling process was conducted to produce the graphite and h-BN composite nanosheets in an ammonia atmosphere.[25] Several grams of a 1:1 graphite and h-BN mixture were added into a steel vial. Acting as a dispersant, 5 wt% oleic acid was injected into the vials for the purpose of enhancing the mechanical exfoliation process and improving the dispersion of the composite nanosheets in oil for subsequent lubrication testing. 25 mm steel balls were loaded in the vial with a ball-to-powder weight ratio of 64:1. The rotating speed was 140 rpm. The vial was sealed and filled with 310 kPa of ammonia (NH_3) gas, which is a critical atmosphere for nanosheet production.[25]

The structure of the synthesised composite nanosheets was examined using X-ray powder diffraction (PANalytical X'pert Powder, Cu *K*-alpha radiation, $\lambda = 0.15418$ nm). A scanning electron microscope (Hitachi S4500 Zeiss Supra 55VP) and a transmission electron microscope (JOEL JEM-2100F) were used to characterize the morphologies and structures of composite nanosheets. To examine the synthesized composite chemical composition, electron energy loss spectroscopy (EELS), and energy-filtered transmission electron microscopy (EFTEM) were performed using a Gatan Quantum ER 965 Imaging Filter attached to a JEOL JEM-2100F instrument. EELS spectra were acquired in the imaged-coupled mode (TEM was in diffraction mode with an area of interest defined by a selected area diffraction aperture), and the elemental maps were acquired using the three-window method.

The tribology testing of the composite nanosheets was carried out via a MRS-10A four-ball wear tester (Jinan Shidai Shijin Testing Machine Group Co., LTD. China), according to the National Standard of the People's Republic of China GB/T 12583-1998 "Standard test method for measurement of extreme-pressure properties of lubrication fluids (four-ball method)", which is equivalent to the standard ASTM D2783-88. The composite nanosheets were dispersed by stirring and ultrasonication in mineral base oil (500 N mineral base oil produced by China Daqing petrochemical company, whose viscosity is 10–12 cSt at 100 °C, pour point −12 °C, flash point 230 °C, Aromatics less than 1 wt%). Four 12.7 mm diameter steel balls made of GCr15 bearing steel (AISI-52100) with the hardness of 64-66 HRC, Grade 25 EP (Extra Polish) were used for testing. The measurement of scar diameters in our experiments was performed following the standard procedure ASTM D2783-88. The balls were left clamped in the cup and washed using cleaning solvent and rinse solvent. The scar diameters of the three test balls were measured under an optical microscope; an average scar diameter was obtained from several measurements in different directions. An ocular micrometer equipped with a calibrated measuring scale (±0.01 mm) was used to determine the average wear scar diameter on the three lower ball, and repeat each test three times at each load and take the mean to eradicate any discrepancies. During the test, the rotating speed of the main spindle was maintained at 1770 rpm, a timer with the accuracy of 0.1 s was employed and the testing temperature was ambient 25 °C. The wear scars were observed using an optical microscope (Leica DMI 3000M).

Acknowledgement

Authors would like to thank the financial support from Australian Research Council under the Discovery scheme.

Conflict of Interest

The authors declare no conflict of interest.

Keywords

ball milling, boron nitride, composite nanosheet, graphene, lubrication

Received: June 6, 2017
Revised: September 15, 2017
Published online: September 29, 2017

[1] K. S. Novoselov, A. K. Geim, S. Morozov, D. Jiang, Y. Zhang, S. A. Dubonos, I. Grigorieva, A. Firsov, *Science* **2004**, *306*, 666.
[2] C. Lee, X. Wei, J. W. Kysar, J. Hone, *Science* **2008**, *321*, 385.
[3] A. A. Balandin, S. Ghosh, W. Bao, I. Calizo, D. Teweldebrhan, F. Miao, C. N. Lau, *Nano Lett.* **2008**, *8*, 902.
[4] L. Boldrin, F. Scarpa, R. Chowdhury, S. Adhikari, *Nanotechnology* **2011**, *22*, 505702.
[5] K. Watanabe, T. Taniguchi, H. Kanda, *Nat. Mater.* **2004**, *3*, 404.
[6] A. Castellanos-Gomez, M. Poot, G. A. Steele, H. S. van der Zant, N. Agraït, G. Rubio-Bollinger, *Adv. Mater.* **2012**, *24*, 772.
[7] A. Splendiani, L. Sun, Y. Zhang, T. Li, J. Kim, C. Y. Chim, G. Galli, F. Wang, *Nano Lett.* **2010**, *10*, 1271.
[8] L. H. Li, J. Cervenka, K. Watanabe, T. Taniguchi, Y. Chen, *ACS Nano* **2015**, *8*, 1457.
[9] L. H. Li, E. J. Santos, T. Xing, E. Cappelluti, R. Roldán, Y. Chen, K. Watanabe, T. Taniguchi, *Nano Lett.* **2015**, *15*, 218.
[10] L. H. Li, Y. Chen, *Adv. Funct. Mater.* **2016**, *26*, 2594.
[11] Q. Cai, A. Du, G. Gao, S. Mateti, B. C. Cowie, D. Qian, S. Zhang, Y. Lu, L. Fu, T. Taniguchi, *Adv. Funct. Mater.* **2016**, *26*, 8202.
[12] W. Lei, S. Qin, D. Liu, D. Portehault, Z. Liu, Y. Chen, *Chem. Commun.* **2013**, *49*, 352.
[13] J. Taha-Tijerina, T. N. Narayanan, G. Gao, M. Rohde, D. A. Tsentalovich, M. Pasquali, P. M. Ajayan, *ACS Nano* **2012**, *6*, 1214.
[14] W. Lei, V. N. Mochalin, D. Liu, S. Qin, Y. Gogotsi, Y. Chen, *Nat. Commun.* **2015**, *6*, 8849.
[15] Q. Cai, S. Mateti, W. Yang, R. Jones, K. Watanabe, T. Taniguchi, S. Huang, Y. Chen, L. H. Li, *Angew. Chem.* **2016**, *128*, 8545.
[16] D. Deepika, L. H. Li, A. M. Glushenkov, S. K. Hait, P. Hodgson, Y. Chen, *Sci. Rep.* **2014**, *4*, 7288.
[17] Y. Kimura, T. Wakabayashi, K. Okada, T. Wada, H. Nishikawa, *Wear* **1999**, *232*, 199.

[18] K. Hu, M. Liu, Q. Wang, Y. Xu, S. Schraube, X. Hu, *Tribol. Int*. **2009**, *42*, 33.
[19] J. Lin, L. Wang, G. Chen, *Tribol. Lett*. **2011**, *41*, 209.
[20] L. Reyes, A. Loganathan, B. Boesl, A. Agarwal, *Tribol. Lett*. **2016**, *64*, 41.
[21] H. Huang, J. Tu, L. Gan, C. Li, *Wear* **2006**, *261*, 140.
[22] R. M. Yunus, H. Endo, M. Tsuji, H. Ago, *Phys. Chem. Chem. Phys*. **2015**, *17*, 25210.
[23] X. Xie, Z. Ao, D. Su, J. Zhang, G. Wang, *Adv. Funct. Mater*. **2015**, *25*, 1393.
[24] C. R. Dean, A. F. Young, I. Meric, C. Lee, L. Wang, S. Sorgenfrei, K. Watanabe, T. Taniguchi, P. Kim, K. Shepard, J. Hone, *Nat. Nanotechnol*. **2010**, *5*, 722.
[25] T. Xing, S. Mateti, L. H. Li, F. Ma, A. Du, Y. Gogotsi, Y. Chen, *Sci. Rep*. **2016**, *6*, 35532.
[26] M. Yi, Z. Shen, *J. Mater. Chem. A* **2015**, *3*, 11700.
[27] Y. Chen, J. F. Gerald, L. T. Chadderton, L. Chaffron, *Appl. Phys. Lett*. **1999**, *74*, 2782.
[28] L. H. Li, Y. Chen, G. Behan, H. Zhang, M. Petravic, A. M. Glushenkov, *J. Mater. Chem*. **2011**, *21*, 11862.
[29] T. Xing, L. H. Li, L. Hou, X. Hu, S. Zhou, R. Peter, M. Petravic, Y. Chen, *Carbon* **2013**, *57*, 515.
[30] Z. Chen, X. Liu, Y. Liu, S. Gunsel, J. Luo, *Sci. Rep*. **2015**, *5*, 12869.
[31] R. Rosentsveig, A. Gorodnev, N. Feuerstein, H. Friedman, A. Zak, N. Fleischer, J. Tannous, F. Dassenoy, R. Tenne, *Tribol. Lett*. **2009**, *36*, 175.
[32] K. Lee, Y. Hwang, S. Cheong, Y. Choi, L. Kwon, J. Lee, S. H. Kim, *Tribol. Lett*. **2009**, *35*, 127.
[33] D. H. Cho, J. S. Kim, S. H. Kwon, C. Lee, Y. Z. Lee, *Wear* **2013**, *302*, 981.
[34] A. Falin, Q. Cai, E. J. Santos, D. Scullion, D. Qian, R. Zhang, Z. Yang, S. Huang, K. Watanabe, T. Taniguchi, M. R. Barnett, Y. Chen, R. S. Ruoff, L. H. Li, *Nat. Commun*. **2017**, *8*, 15815.
[35] I. Leven, D. Krepel, O. Shemesh, O. Hod, *J. Phys. Chem. Lett*. **2013**, *4*, 115.

